Adsorption of Atomic Hydrogen at a Nanostructured Electrode of Polyacrylate-Capped Pt Nanoparticles in Polyelectrolyte

Marie Zabel Markarian, Maysaa El Harakeh, and Lara I. Halaoui*

Chemistry Department, The American University of Beirut, Beirut 110236, Lebanon

Received: December 16, 2004; In Final Form: April 16, 2005

Atomic hydrogen electrosorption is reported at crystallite sites of polyacrylate-capped Pt nanoparticles ($\langle d \rangle = 2.5 \pm 0.6$ nm), by assembling nanostructured electrodes of polyacrylate−Pt nanocrystallites layer-by-layer in a cationic polyelectrolyte, poly(diallyldimethylammonium chloride). Cyclic voltammetry in 1 M H_2SO_4 revealed a strongly adsorbed hydrogen state and a weakly adsorbed hydrogen state assigned to adsorption at (100) and (110) sites of the modified nanocrystallites, respectively. Resolving hydrogen adsorption states signifies that surface capping by the carboxylate groups is not irreversibly blocking hydrogen adsorption sites at the modified Pt nanoparticle surface. Adsorption peak currents increased with increasing the number of layers up to 16 bilayers, indicating the feasibility of nanoparticle charging via interparticle charge hopping and the accessibility of adsorption states within the thickness of the nanoparticle/polyelectrolyte multilayers. Despite similarity in hydrogen adsorption in the cyclic voltammorgrams in 1 M H_2SO_4, negative shifts in adsorption potentials were measured at the nanocrystallite Pt−polyelectrolyte multilayers relative to a polycrystalline bulk Pt surface. This potential shift is attributed to a kinetic limitation in the reductive hydrogen adsorption as a result of the Pt nanoparticle surface modification and the polyelectrolyte environment.

Introduction

Pt is a catalyst for a number of significant reactions, including hydrogen evolution, oxygen reduction, hydrogen oxidation, methanol oxidation, and hydrogenation reactions.[1−4] Reducing the size of the catalyst to the nanoscale[5] results in increasing the number of catalytic sites per unit mass and may be coupled with a crystallite-size effect increasing the turnover number with decreased dimensionality for some structure-sensitive reactions.[1]

Recent developments in synthesizing Pt nanoparticles with surface capping agents[6−8] permitted control over the nanoparticle size, shape, and crystallinity and therefore opened the possibility for systematic studies of nanoscale catalysis. For example, polyacrylate-capped Pt nanocrystallites have been synthesized in cubic, tetrahedral, and octahedral shapes and in varied sizes by El-Sayed and co-workers.[6] In addition to kinetically trapping the particle in nanometer dimensions, surface modifiers can form a basis of interactive forces for nanoparticle transfer to surfaces. We have thus assembled polyacrylate (PAC)-capped Pt nanocrystallites as multilayers in poly(diallyldimethylammonium chloride).[9] This assembly, driven by electrostatic and hydrophobic interactions between the nanoparticles capped with an anionic polyelectrolyte and a cationic polyelectrolyte, may offer a facile method for designing high-surface-area heterogeneous catalysts (and electrocatalysts) from mixtures of nanoparticles, provided that the modified nanoparticles retain their surface catalytic activity and that the polyelectrolyte multilayer matrix does not present an insurmountable barrier to charge hopping or mass transport in the assemblies.

In this paper, nanostructured electrodes of polyacrylate-capped Pt nanoparticles of $\langle d \rangle = 2.5$ nm $\pm$ 0.6 nm assembled in poly(diallydimethylammonium chloride) are utilized to probe the underpotential deposition of atomic hydrogen at the modified Pt nanocrystallites.

The underpotential deposition of atomic hydrogen H_{upd} is a structure-sensitive catalytic process characteristic of the Pt surface, reported at Pt(100), Pt(110), and Pt(111) single crystals, polycrystalline Pt, Pt black, and high-surface-area Pt on carbon.[10−14] We report here the observation of the electrosorption of atomic hydrogen at crystallite sites of PAC−Pt nanoparticles and compare hydrogen adsorption at the nanostructured Pt electrode to H_{upd} at a polycrystalline Pt surface. Negative shifts in adsorption potentials were measured relative to an activated polycrystalline Pt surface and are attributed to a reductive adsorption activation rather than to a mass-transport limitation or a charge transport limiting rate. The adsorption peak currents increased linearly with the number of bilayers, up to a certain thickness, indicating the feasibility of charge hopping in nanoparticle−polyelectrolyte multilayers and the accessibility of embedded nanocrystallite adsorption sites. Resolving hydrogen adsorption states at the modified nanoparticles embedded in polyelectrolyte multilayers is believed to be a significant finding because it indicates that surface capping by the carboxylate groups is not blocking H_{upd} catalytic sites.

Experimental Methods

Materials. The following materials were used in this study: potassium hexachloroplatinate(IV), K_2PtCl_6 (Fluka Chemika, ~40% Pt); poly(acrylic acid) 2100 sodium salt, PAC (Fluka Chemika, pH in water 6−8); poly(diallyldimethylammonium chloride), PDDA, 20 wt % in water, average molecular weight ~200 000−350 000 Da, $d = 1.040$ (Aldrich); sodium citrate (AnalaR); sulfuric acid 95−97% (Schalau, reagent grade, ISO, pH eur $d = 1.84$); ammonium hydroxide, 28−30 wt % $d = 0.89$ (ACROS Organics); hydrogen peroxide 30% (GmbH); ethanol 98% (Merck). All aqueous solutions were prepared with

* Author to whom correspondence should be addressed. E-mail: lh07@aub.edu.lb.

10.1021/jp044267m CCC: $30.25
Published on Web 05/21/2005

double-distilled water. The reported concentration of the polymer solution is for the monomer unit.

Pt Nanoparticle Synthesis. The synthesis of the PAC-capped Pt nanoparticles and their layer-by-layer assembly in PDDA have been previously reported.[9] Briefly, 10 mg of K_2PtCl_6 was dissolved in a 50 mL aqueous solution containing 1.34 g of the stabilizing PAC polymer. A solution of 0.50 g of sodium citrate in 50 mL of water was added to reduce the Pt cation, and the (100 mL) mixture was refluxed in an oil bath (120 °C) for 3 h 30 min, yielding a solution of gold brown Pt nanoparticles. This solution is termed *as-prepared*. Transmission electron microscopy (JEOL-2010 high-resolution TEM operated at 200 kV, NHFML, Florida State University) revealed the growth of face-centered cubic (fcc) nanocrystallites of 2.5 ± 0.6 nm in average diameter.[9a]

Layer-by-Layer Assembly Protocol. Polyacrylate-capped Pt nanoparticles were assembled layer-by-layer in polydiallyldimethylammonium chloride (PDDA) on indium-doped tin oxide glass (In/SnO_2 or ITO; Delta Technologies, Ltd., $25 \times 75 \times 1.1$ mm^3 polished float glass surface, coated one side, $R_s = 8-12$ Ω). Prior to film assembly, ITO substrates were cleaned by immersion in boiling ethanol for 10 min, rinsed with water, and dipped for 10 min in warm 7:3 (v/v) NH_3/H_2O_2 aqueous solution. Substrates were then rinsed three times in double-distilled water, 2 min each time, and dried in air or under a nitrogen flow. To assemble PDDA/Pt nanoparticle multilayers on ITO, the electrodes were dipped in 10 mM PDDA/0.4 M NaCl solution for 30 min, rinsed 2×1 min with double-distilled water, and dried in air for 10 min. The PDDA-modified electrodes were then dipped in the as-prepared Pt solution for 1 h, immersed in water for 1 min once, and dried in air for 15 min. A layer of PDDA−Pt is thus formed. This procedure was repeated *n* times using a software-controlled multilayer assembly robot (StratosequenceV, Nanostrata Inc., Tallahassee, FL) to form $(PDDA/Pt)_n$ layers on ITO, where *n* represents the number of bilayers.

Electrochemical Measurements. Electrochemical measurements were acquired in a three-electrode electrochemical cell, with $(PDDA/nano\text{-}Pt)_n$ on ITO or a polycrystalline Pt electrode (5 mm Pt disk or a Pt wire 1 mm in diameter) as the working electrode. A Pt wire served as the counter electrode, and a Ag/AgCl electrode was used as the reference electrode (Analytical Sensors, Inc.). The cross-sectional geometric area of the $(PDDA/Pt)_n$ films was around 2.5 cm^2, was measured following each electrochemical measurement, and accounted for as-measured in reporting current densities. The full electrode area in contact with solution was covered with the PDDA/Pt film.

Cyclic voltammograms were collected with a home-interfaced bipotentiostat (model AFCBP1, Pine Instruments Company) and Pine 2.7 software. Prior to measurements, solutions were deoxygenated by bubbling nitrogen for 30 min, and a nitrogen blanket was maintained above the solution during measurements. A cyclic voltammogram of 5 mM $Fe(CN)_6^{3-}$/5 mM $Fe(CN)_6^{4-}$ in 0.1 M KNO_3 was acquired at an electrochemically activated bulk Pt working electrode (after cycling in 1 M H_2SO_4) before and after electrochemical measurements of hydrogen adsorption, to ensure that the potential of the reference electrode did not shift in the course of measurements in 1 M sulfuric acid.

To obtain the hydrogen adsorption characteristics reported at the polycrystalline Pt electrodes, the Pt (1 mm in diameter wire or 5 mm in diameter disk) working electrode was first electrochemically activated in 1 M H_2SO_4 to create a freshly reduced platinized surface by cycling the potential between 2 and −1 V at a 500 mV/s scan rate for 100 cycles, until the hydrogen adsorption peaks were clearly resolved. However, scanning to these extreme potentials was not performed in the case of the PDDA/Pt nanoparticle multilayers. The potential range for scanning the $(PDDA/Pt)_n$/ITO films was within the range 800 to −150 mV in 1 M H_2SO_4, outside the potential range of Pt oxide formation and reduction. This ensured that atomic hydrogen adsorption sites were identified at the as-prepared capped nanoparticles without subjecting the nanoparticles to known surface restructuring at extreme potentials that may change the as-prepared surface sites and may cause decapping.

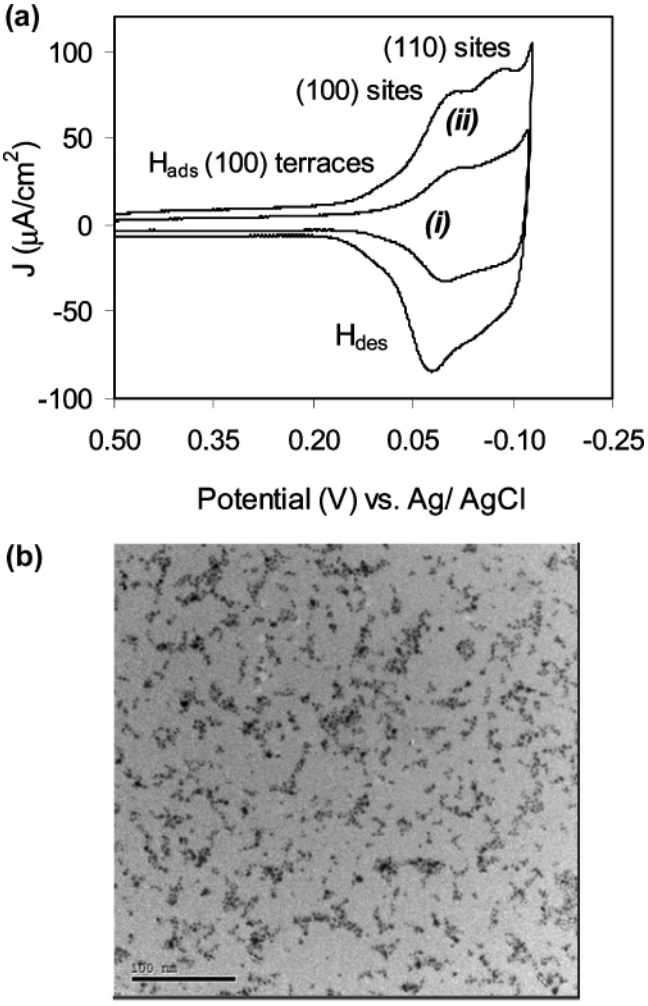

Figure 1. (a) Cyclic voltammograms of (i) 2 bilayers and (ii) 4 bilayers of Pt nanoparticles in PDDA on ITO in deoxygenated 1 M H_2SO_4 electrolyte. The scan rate is 20 mV/s. (b) TEM image of Pt nanoparticles deposited on a layer of PDDA by floating a PDDA-modified SiO−Cu grid for 60 min on the surface of the as-prepared Pt solution. The scale bar is 100 nm.

Results

Multilayers of polyacrylate-capped Pt nanoparticles of $\langle d \rangle = 2.5 \pm 0.6$ nm were assembled layer-by-layer in poly(diallyldimethylammonium chloride), PDDA, on ITO. Figure 1a shows cyclic voltammograms (CVs) at 2 bilayers ($(PDDA/Pt)_2$) and 4 bilayers ($(PDDA/Pt)_4$) acquired at 20 mV/s in 1 M H_2SO_4 showing the adsorption H_{ads} (or H_{upd}) and desorption H_{des} of atomic hydrogen at the Pt nanocrystallite (nano-Pt) surface according to $H^+ + e^-$ (PAC−nano-Pt) → H_{ads}−nano-Pt. Strongly adsorbed H(S) and weakly adsorbed H(W) states were resolved at the nanocrystallite multilayers and are attributed to adsorption at different crystallite sites at the nanoparticle surface.

The H(S) state appeared as a shoulder at −9 to −11 mV, whereas the H(W) state manifested as a rising current at (PDDA/Pt)$_2$ in the potential range −46 to −112 mV, and developed into a peak with E_{peak} = −85 mV at 4 bilayers. Reported electrochemical studies at Pt electrode single crystals, Pt black, and polycrystalline Pt have assigned the strongly adsorbed hydrogen state and the weakly adsorbed hydrogen state to adsorption at (100) and (110) catalytic sites, respectively, as indicated in Figure 1a.[10]

Furthermore, a reduction current in the range of 146 to −62 mV attributed to a long-range adsorption state at (100) terraces[10] was also resolved, which would signify according to such assignment the presence of a long-range order of (100) terraces at the Pt nanoparticle surface.

The adsorbed charge density (for hydrogen adsorption) at 4 bilayers of PDDA/nano-Pt was computed from the $I-V$ curve in the potential range 165 to −115 mV to be equal to 677 μC/cm^2, after accounting for double-layer charging (where the area refers to the geometric electrode area). Comparison with an adsorbed charge density of 210 μC/cm^2 in 1 M H_2SO_4 at room temperature at Pt, corresponding to 1.305×10^{15} atoms/cm^2 and assuming a 1:1 ratio of adsorbed hydrogen atom per Pt atom, reveals that a 4-bilayer PDDA/nano-Pt film adsorbs 3.2 times as many H atoms as a real polycrystalline Pt surface of the same geometric area. If one considers, for the purpose of the calculation, a closely packed cubic assembly of spherical Pt nanoparticles of 2.5 nm in diameter (and assumes 3 Å for the organic cap, i.e., a 1.5-Å-thick shell, giving a diameter of 2.8 nm), then one finds that the measured charge density at (PDDA/Pt)$_4$ is equivalent to 1 fully active closely packed monolayer and 0.3 of a monolayer (coverage = 1.3) of Pt nanoparticles 2.5 nm in diameter/0.3 nm PAC. TEM images revealed that a 60 min dipping of a PDDA-primed surface in Pt nanoparticle solution (one layer of Pt) results in submonolayer coverage of Pt on PDDA (cf. Figure 1b, ref 9a). Considering the low surface coverage per layer imaged by TEM, that the nanoparticles are capped with polyacrylate, and that modifying a bulk Pt surface by dipping in a polyacrylate solution resulted in blocking its hydrogen adsorption states in the cyclic voltammogram in 1 M H_2SO_4 (results not shown), the high magnitude of adsorbed charge density at (PDDA/Pt)$_4$ appears as a significant result indicating an appreciable catalytic surface activity of surface-modified Pt nanoparticles toward hydrogen adsorption.

The magnitude of adsorbed charge density (attributed to adsorption at (100) and (110) sites and (100) terraces) increased linearly with the number of bilayers (up to $n = 16$), in agreement with the linear increase in nanoparticle density per bilayer measured by UV−vis absorption.[9a] Peak current (i_p) densities corresponding to H(S) and H(W) states also increased almost linearly ($R^2 = 0.985$) with the number of layers up to 16 bilayers (cf. inset of Figure 2 for H(W) i_p at 20 mV/s), indicating the feasibility of nanoparticle charging in layers away from the electrode surface likely via interparticle charge hopping. The linear increase in i_p with n also indicates the accessibility and activity of adsorption states at nanoparticles buried within the polyelectrolyte multilayer thickness.

Figure 2 shows a CV in 1 M H_2SO_4 acquired at 20 mV/s at (PDDA/Pt)$_{14}$ where the adsorption potentials are shown to be negatively shifted compared to the CVs at (PDDA/Pt)$_2$ and (PDDA/Pt)$_4$. The adsorption of atomic hydrogen assigned to (100) sites occurred between 16 and −94 mV (shoulder at −47 mV), and E_{peak} for adsorption attributed to (110) sites was measured at −145 mV. As such, H(W) and H(S) adsorption

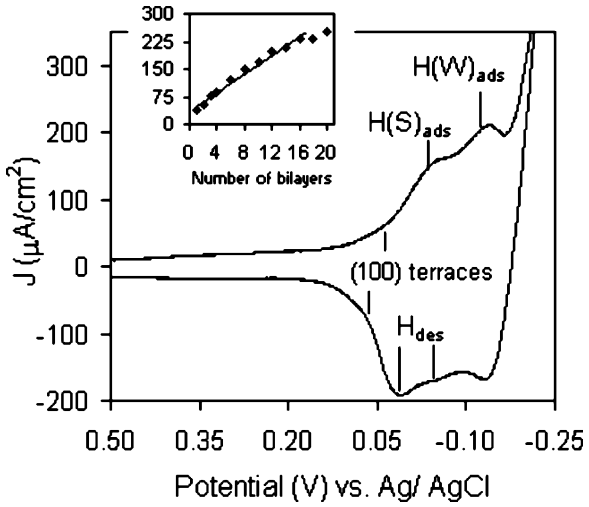

Figure 2. Cyclic voltammogram of 14 bilayers of PDDA/nano-Pt on ITO in deoxygenated 1 M H_2SO_4 electrolyte. Scan rate is 20 mV/s. The inset shows a H(W) peak current density at 20 mV/s as a function of the number of PDDA/Pt bilayers.

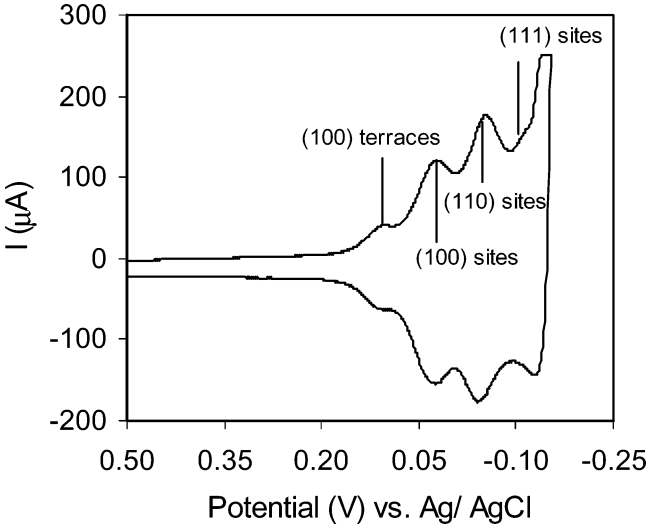

Figure 3. CV of an electrochemically activated polycrystalline Pt wire in deoxygenated 1 M H_2SO_4 electrolyte. The scan rate is 100 mV/s.

are negatively shifted by 60 and 38 mV, respectively, at 14 bilayers relative to 4 bilayers. The onset of long-range adsorption at (100) terraces was similarly shifted by approximately −53 mV compared to (PDDA/Pt)$_4$. This negative potential shift is attributed to an additional activation overpotential with an increased number of layers, as discussed below, even though all sites in the multilayers remain equally active (and accessible) for hydrogen adsorption in this time scale.

The underpotential deposition at atomic hydrogen at PDDA/Pt multilayers was compared to hydrogen electrosorption at a polycrystalline Pt electrode (polycryst-Pt) to elucidate the effect of the polyelectrolyte−nanoparticle film architecture, i.e., the nanoparticle environment and surface modification. Despite similarity in the CVs in 1 M H_2SO_4 at the two Pt surfaces, the hydrogen adsorption potentials were negatively shifted at the multilayers relative to the bulk Pt electrode, even at films as thin as 2 bilayers of PDDA/Pt. A typical CV of an electrochemically activated Pt wire (1 mm in diameter) in 1 M H_2SO_4 is presented in Figure 3, showing E_{peak} for H(S) and H(W) states at 16 and − 60 mV, respectively, and E_{peak} adsorption at (100) terraces at 101 mV (range of 177−78 mV). Also observed in

TABLE 1: Comparison of Hydrogen Adsorption and Desorption Potentials at the Nanocrystalline Pt Films and Polycrystalline Pt

	H(S), E(mV ± 5 mV)				H(W), E(mV ± 5 mV)	
	range H_{ads}	E_{peak} H_{ads}	E_{peak} H_{des}	ΔE_p	range H_{ads}	E_{peak} H_{ads}
poly Pt	78, −15	16	28	12	15, −96	−60
$(PDDA/Pt)_4$	62, −40	−9	27	36	−40,−111	−85
$(PDDA/Pt)_{14}$	16, −94	−47	26	73	−94, −171	−145

this $I-V$ curve is a rising current attributed in the literature to (long-range) adsorption at (111) sites,[10,12b] which was not resolved at the nanocrystals.

There are several marked differences between the current−potential response at the nanocrystallite films and the polycrystalline Pt electrode. (1) Peak potentials for H_{upd} are negatively shifted at the nanocrystallite films, a shift which increased with increasing the number of bilayers (−25 and −63 mV shifts for H(S) at $(PDDA/Pt)_4$ and $(PDDA/Pt)_{14}$, respectively; cf. polycryst-Pt). (2) H_{des} took place at essentially the same potential at polycrystalline Pt and the nanostructured films when measured at 20 mV/s (at ∼27 mV; cf. Table 1). (3) The adsorption−desorption peaks at polycryst-Pt appear as almost mirror images whereas the peak separation ΔE_{peak}, resulting mainly from the shift in the cathodic peaks at a scan rate of 20 mV/s, is wide at the multilayers and increases with an increasing number of bilayers (cf. Table 1).

Furthermore, a linear increase in peak current with ν was measured at the bulk polycrystalline Pt electrode as expected for a facile surface charge transfer, while deviation from this linear dependence (of i_p on ν) occurred at scan rates higher than 500 mV/s at 2 bilayers, indicating the onset of the effect of a slow rate-determining process. At 14 bilayers, the linear dependence of i_p on ν could only be measured up to 50−100 mV/s. Figure 4a shows hydrogen adsorption peak current density (H(S) state) versus the scan rate ν at $(PDDA/Pt)_2$, $(PDDA/Pt)_{14}$, and a Pt disk electrode (5 mm in diameter).

The adsorption peak potential $E_{p,c}$ also shifted negatively with increasing ν at the PDDA/Pt multilayers, whereas $E_{p,c}$ at the polycrystalline Pt electrode was independent of the scan rate (measurement for ν up to 1 V/s). The shifts in the cathodic peak potential, namely, $\Delta E_{p,c}$, measured with reference to the peak potential at slow scan rate (1−5 mV/s) for each surface, are presented in Figure 4b for 2 bilayers, 14 bilayers, and polycrystalline Pt, further corroborating the presence of an additional resistance in one of the determining rates toward hydrogen adsorption. This shift is observed at films as thin as 2 bilayers of PDDA/Pt and increased with increasing the number of bilayers.

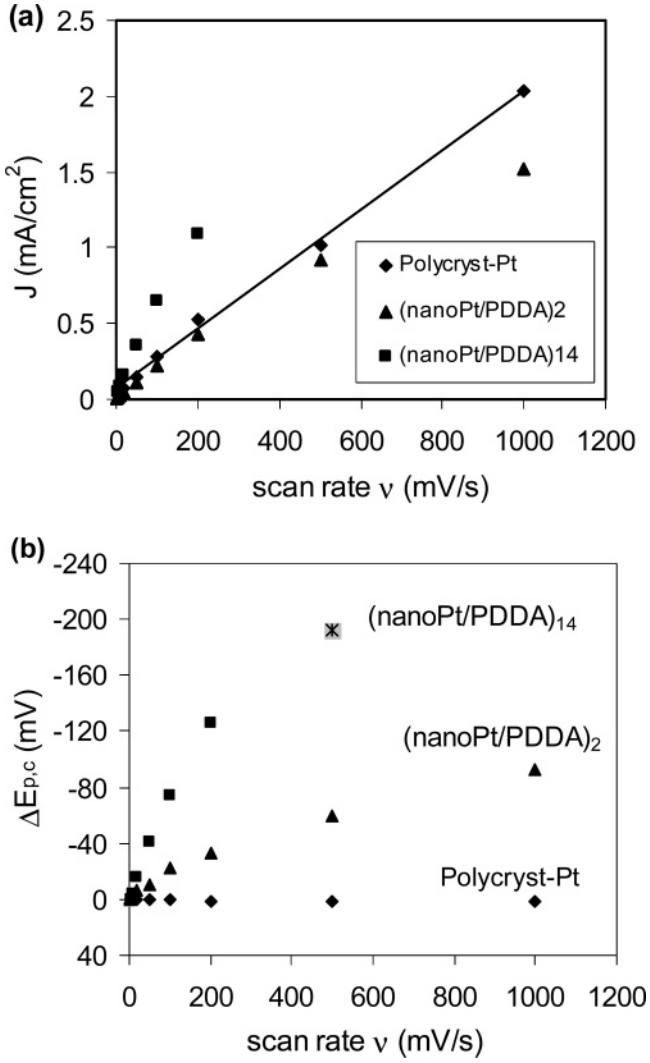

Figure 4. (a) Peak current densities at $(PDDA/Pt)_2$, $(PDDA/Pt)_{14}$, and a Pt disk electrode (5 mm in diameter, polycryst-Pt) vs the scan rate. The linear dependence of J on ν at polycryst-Pt is shown. (b) Plots of shifts in cathodic peak potentials, $\Delta E_{p,c}$ ($=E_{p,c}(\nu) - E_{p,c}$ (1 or 5 mV/s) for each electrode surface), measured at $(PDDA/Pt)_2$, $(PDDA/Pt)_{14}$, and a Pt disk electrode vs ν. The point marked by × for $(PDDA/Pt)_{14}$ denotes an inaccurate determination to show that the peaks are no longer resolved at these scan rates. The supporting electrolyte is 1 M H_2SO_4.

Discussion

Mirror-imaged peaks in a cyclic voltammogram are diagnostic of a reversible surface charge-transfer process,[13,14] here a quasi-equilibrium $H^+ + e^-(Pt) \leftrightarrow H_{ads}-Pt$ at the activated bulk Pt electrode. Appreciable peak separation at the modified Pt nanoparticles assembled in the cationic polyelectrolyte indicates the introduction of a kinetically sluggish step in the charge-transfer mechanism leading to adsorption of atomic hydrogen. The cause of the negative potential shift of atomic hydrogen adsorption cannot be of thermodynamic nature, because then both the anodic and cathodic peaks should shift in the same direction, which was not observed.

The underpotential deposition of atomic hydrogen at the modified Pt nanocrystallite sites necessitates at first film charging to achieve a nanocrystallite electron electrochemical potential favorable for charge transfer. Nanoparticle charging is assumed to take place via charge hopping through interparticle distances (possibly facilitated by the presence of transport pathways created by layer interpenetration), driven by an electrochemical potential gradient. Upon an (equilibrium) electrochemical potential favorable for charge transfer to protons in the polyelectrolyte multilayers being reached, electron transfer at the nano-Pt surface takes place followed by adsorption of atomic hydrogen at a Pt adsorption site. Because the nanoparticles are modified and embedded in the polyelectrolyte matrix, it is envisioned that this step must be followed by surface (and solvent term) reorganization as hydrogen adsorbs on the catalytic site (Scheme 1). Ion transport in the multilayered film accompanies the charge-transfer process to maintain the PDDA/Pt film electroneutrality (mainly by transport of H^+ in the film and to a lesser extent of the anionic counterion by hopping or through channels).

Mass transport in polyelectrolyte multilayers (PEMs) and the electrochemical response of PEM-modified electrodes have been

SCHEME 1: Sketch of Multilayers of Polyacrylate-Capped Pt Nanoparticles Assembled Layer-by-Layer in a Cationic Polyelectrolyte, PDDA, on ITO[a]

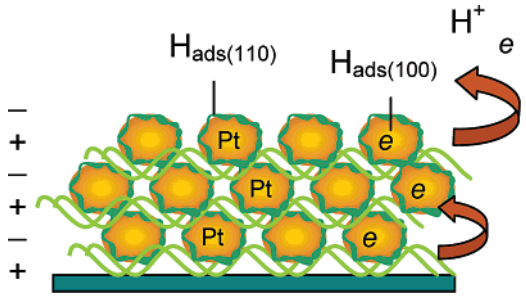

[a] The scheme shows film charging via charge hopping, followed by electron transfer to H^+ and adsorption of atomic hydrogen at (110) and (100) adsorption sites of the Pt nanocrystallites. Adsorbed atomic hydrogen is referred to as $H_{ads(110)}$ or $H_{ads(100)}$, in reference to these adsorption states, respectively.

investigated in a number of reports.[15−24] The permeability of polyelectrolyte multilayers and the electrochemical response of PEM-modified electrodes to redox systems will depend to a great extent on the type of adsorbed polyelectrolytes, the deposition parameters (e.g., ionic strength during assembly), the nature and charge of the redox couple, and the charge of the outermost layer. Polyelectrolyte multilayers have been shownto exhibit high permeability to monovalent ions and exclusion of multivalent ions, with the permeability decreasing with an increased number of layers.[19] The Donnan exclusion of ions having the same surface charge as the outermost layer and the Donnan enhancement of the concentration of ions bearing an opposite charge have been observed and form a selectivity basis in these membranes. A capillary membrane model has been proposed recently to model mass transport in PEMs, showing good agreement with impedance measurements on systems of polystyrenesulfonate/polypeptides.[15] Schlenoff et al. had also addressed mass transport in these films and proposed an ion-hopping mechanism between exchange sites in the multilayers, sites that are created by the salt in solution.[16−18]

Although the nanoparticle−polyelectrolyte system studied here is different from systems thus described, the same mass-transport principles are expected to remain in effect. However, in addition to ion transport in the multilayers, charge transfer at the surface of the Pt nanoparticles embedded in the polyelectrolyte and surface adsorption−desorption processes will also dictate the rate of electrosorption of hydrogen at the modified nanocrystallites in the multilayers.

Several rates are summed to govern the mechanism leading to hydrogen adsorption at the nanostructured Pt−polyelectrolyte electrode: (1) the electron hopping rate (or charge hopping resistance R_{ch}), (2) mass transport of protons coupled with counterion transport, to bring the electrochemically active species to the nano-Pt adsorption sites and to preserve the film electroneutrality (mass transfer resistance R_{mt}), and (3) the kinetics of charge transfer and adsorption of hydrogen at the polyacrylate-modified Pt nanoparticles, where the carboxylate oxygen atoms are thought to be adsorbed (charge-transfer resistance R_{ct}).

The negative shift in $E_{p,c}$ at the nanocrystallite multilayers at slow scan rates relative to the polycryst-Pt surface is unlikely to have resulted from a slow charge hopping rate or a high R_{mt}. A high R_{ch} should be manifested in comparable shifts in $E_{p,c}$ and $E_{p,a}$ in opposite directions, which was not the case at a slow scan rate (20 mV/s), as hydrogen desorption peak potentials $E_{p,a}$ remained essentially invariant (cf. Table 1). Similarly, a high R_{mt} in the multilayers causing $E_{p,c}$ to shift negatively while not affecting $E_{p,a}$ is not physically plausible. The process of reductive adsorption $H^+ + e^- \rightarrow H_{ads}$ at the nanoparticles is accompanied by proton transport into the multilayers and transport of HSO_4^- and SO_4^{2-} counterions to solution to maintain electroneutrality. Mass transport should not be especially hindered for this cathodic process considering the multilayers' negative surface charge (Pt nanoparticles as the outermost layer) and their high permeability to the monovalent H^+ cation (coupled with the Donnan exclusion of anions). However, a high R_{mt} may be expected to cause $E_{p,a}$ for the oxidative desorption to shift in the positive direction because of such Donnan exclusion of anions and selectivity for protons. The absence of this effect is probably due to the high ionic strength of the acid solution.

We also find that modifying the electrode (ITO) with only 2 bilayers of PDDA/nano-Pt does not cause a shift in $E_{p,c}$ and $E_{p,a}$ for 5 mM $Fe(CN)_6^{3-}$/5 mM $Fe(CN)_6^{4-}$ in 0.1 M KNO_3 relative to an unmodified electrode (likely because of low surface coverage), while a potential shift for hydrogen adsorption almost equal to that measured at 4 bilayers is measured at 2 bilayers (Figure 1a). This presents further evidence that the observed shift in $E_{p,c}$ for hydrogen adsorption with respect to the polycrystalline electrode is not due to a mass-transport resistance at a slow scan rate (20 mV/s). At higher scan rates, the cathodic and anodic peak potentials $E_{p,c}$ and $E_{p,a}$ shift in opposite directions, which can be attributed to charge hopping and mass-transport limitations.

Accordingly, the negative shift in $E_{p,c}$ at slow scan rates at the PDDA/nanoparticle multilayers compared to polycryst-Pt is ascribed to a kinetic limitation in the reductive adsorption at the modified surface, as a result of a different local Pt surface environment (polyacrylate-capped nanoparticles assembled in the cationic polyelectrolyte), and thus a different local proton environment. It is conceivable that higher reorganization energy for charge transfer and adsorption or a limitation due to a smaller probability of electronic tunneling at the modified surface decreasing the rate constant results in an additional activation barrier for the forward rate. As the number of multilayers increased, differences in the local environments as a result of variations in multilayer structure may have caused the additional shift in cathodic peak potentials. Separating the effect of nanocrystallite size on the adsorption kinetics from these factors is not possible in the absence of a study of similarly modified and assembled nanoparticles of different sizes and shapes, a study that is in progress.

Conclusions

Hydrogen adsorption states were observed at as-prepared polyacrylate-capped Pt nanoparticles assembled in a cationic polyelectrolyte on electrode surfaces, without subjecting the nanoparticle surface to surface restructuring or decapping. The featured strong hydrogen adsorption state and weak hydrogen adsorption state, assigned to different crystallite sites at the modified nanoparticles, were resolved in the cyclic voltammograms in sulfuric acid. At the nanostructured surfaces, the adsorption peak currents increased linearly with the number of bilayers, up to a certain thickness, indicating the feasibility of charge hopping in nanoparticle−polyelectrolyte multilayers and the accessibility of embedded nanocrystallite adsorption sites. In comparison to a polycrystalline Pt electrode, the capped nanoparticles were shown to exhibit significant surface catalytic activity for this process. Resolving hydrogen adsorption states at the modified nanoparticles signifies that surface capping by

the carboxylate groups is not blocking the surface catalytic sites, which opens possibilities for catalysis and electrocatalysis at well-characterized and modified Pt nanocrystallites.

Acknowledgment. We thank Dr. Yan Xin at NHMFL, Florida State University, for acquiring the TEM image (under cooperative agreement DMR-0084173 and NSF grant no. DMR-9625692). Acknowledgment is made to the donors of the American Chemical Society Petroleum Research Fund (PRF #40548-B10) and to the American University of Beirut University research board (URB, grant 2002−2004) for financial support of this research.

Note Added after ASAP Publication. This article was published ASAP on May 21, 2005. In paragraph five of the Results section, some of the data referring to Figure 2 has been revised. The correct version was posted on May 25, 2005.

References and Notes

(1) Marković, N. M.; Radmilovic, V.; Ross, P. N., Jr. In *Catalysis and Electrocatalysis at Nanoparticle Surfaces*; Wieckowski, A., Savinova, E. R., Vayenas, C. G., Eds.; Marcel Dekker: New York, 2003; Chapter 9.

(2) Liu, Z.; Ling, X. Y.; Su, X.; Lee, J. Y. *J. Phys. Chem. B* **2004**, *108*, 8234.

(3) (a) Yoo, J.-W.; Hathcock, D.; El-Sayed, M. *J. Phys. Chem. A* **2002**, *106*, 2049. (b) Cocco, G.; Campostrini, R.; Cabras, M. A.; Carturan, G. *J. Mol. Catal.* **1994**, *94*, 299. (c) Otero-Schipper, P. H.; Wachter, W. A.; Butt, J. B.; Burwell, R. L.; Cohen, J. B. *J. Catal.* **1997**, *50*, 494.

(4) Marković, N. M.; Gasteiger, H. A.; Ross, P. N., Jr. *J. Phys. Chem.* **1995**, *99*, 3411.

(5) (a) Eppler, A.; Rupprechter, G.; Guzi, L.; Somorjai, G. A. *J. Phys. Chem.* **1997**, *101*, 9973. (b) Thomas, J. M.; Johnson, B. F. G.; Raja, R.; Sankar, G.; Midgley, P. A. *Acc. Chem. Res.* **2003**, *36*, 20.

(6) (a) Ahmadi, T. S.; Wang, Z. L.; Green, T. C.; Henglein, A.; El-Sayed, M. A. *Science* **1996**, *272*, 1924. (b) Ahmadi, T. S.; Wang, Z. L.; Henglein, A.; El-Sayed, M. A. *Chem. Mater.* **1996**, *8*, 1161. (c) Petrovski, J. M.; Wang, Z. L.; Green, T. C.; El-Sayed, M. A. *J. Phys. Chem. B* **1998**, *102*, 331.

(7) (a) Li, Y.; Hong, X. M.; Collard, D. M.; El-Sayed, M. A. *Org. Lett.* **2000**, *2*, 2385. (b) Li, Y.; Boone, E.; El-Sayed, M. A. *Langmuir* **2002**, *18*, 4921.

(8) Toshima, N.; Yonezawa, T.; Kushihashi, K. *J. Chem. Soc., Faraday Trans.* **1993**, *89*, 2537.

(9) (a) Ghannoum, S.; Xin, Y.; Jaber, J.; Halaoui, L. I. *Langmuir* **2003**, *19*, 4804. (b) Markarian, M. Z.; El-Harakeh, M.; Makki, R. *Mater. Res. Soc. Symp. Proc.* **2004**, *882*, S8.8−S8.13.

(10) Clavilier, J. In *Electrochemical Surface Science: Molecular Phenomena at Electrode Surfaces*; Soriaga, M. P., Ed.; ACS Symposium Series 378; American Chemical Society: Washington, DC, 1988; p 202.

(11) Will, F. G. *J. Electrochem. Soc.* **1965**, *112*, 451.

(12) (a) Duarte, M. Y.; Martins, M. E.; Arvia, A. *J. Electrochim. Acta* **1980**, *25*, 1613. (b) Kita, H.; Ye, S.; Aramata, A.; Furuya, N. *J. Electroanal. Chem.* **1990**, *295*, 317. (c) Ye, S.; Kita, H.; Aramata, A. *J. Electroanal. Chem.* **1992**, *333*, 299. (d) Kinoshita, K.; Ferrier, D. R.; Stonehart, P. *Electrochim. Acta* **1978**, *23*, 45.

(13) Gómez, R.; Orts, J. M.; Álvarez-Ruiz, B.; Feliu, J. M. *J. Phys. Chem. B* **2004**, *108*, 228.

(14) Bard, A. J.; Faulkner, L. R. *Electrochemical Methods: Fundamentals and Applications*, 2nd ed.; John Wiley & Sons: New York, 2001; Chapters 13 and 14.

(15) Barreira, S. V. P.; Garcia-Morales, V.; Pereira, C. M.; Manzanares, J. A.; Silva, F. *J. Phys. Chem. B* **2004**, *108*, 17973.

(16) Farhat, T. R.; Schlenoff, J. B. *Langmuir* **2001**, *17*, 1184−1192.

(17) Farhat, T. R.; Schlenoff, J. B. *J. Am. Chem. Soc.* **2003**, *125*, 4627−4636.

(18) Rmaile, H. H.; Farhat, T. R. *J. Phys. Chem. B* **2003**, *107*, 14401−14406.

(19) Krasemann, L.; Tieke, B. *Langmuir* **2000**, *16*, 287.

(20) Lebedev, K.; Ramírez, P.; Mafé, S.; Pellicer, J. *Langmuir* **2000**, *16*, 9941.

(21) Antipov, A. A.; Sukhorukov, G. B.; Möhwald, H. *Langmuir* **2003**, *19*, 2444.

(22) Han, S.; Lindholm-Sethson, B. *Electrochim. Acta* **1999**, *45*, 845.

(23) Harris, J. J.; Bruening, M. L. *Langmuir* **2000**, *16*, 2006.

(24) Pardo-Yissar, V.; Katx, E.; Lioubashevski, O.; Willner, I. *Langmuir* **2001**, *17*, 1110−1118.